Electronic Supplementary Information

Rate-controlled nano-layered assembly mechanism of melamine-induced melamine-uric acid stones and its inhibition and elimination methods

Wenya Dong,[a] Yuzhen Zhang,[a] Ping Hu,*[b] Hongwu Xu,[a] Jie Fan,[c] Jiansheng Su,[a] Fang Li,[a] Yun Chen,[a] Ping Li,[a] Shilong Wang,[a] Fredric L. Coe*[d] and Qingsheng Wu*[a]

[a] *School of Chemical Science and Engineering; School of Stomatology; Shanghai First Maternity and Infant Hospital; School of Life Science and Technology; Shanghai Key Laboratory of Chemical Assessment and Sustainability, Tongji University, Shanghai 200092, P. R. China. E-mail: qswu@tongji.edu.cn*

[b] *State Key Laboratory of High Performance Ceramics and Superfine Microstructures, Shanghai Institute of Ceramics, Chinese Academy of Sciences, Shanghai 200050, P. R. China. E-mail: huping@mail.sic.ac.cn*

[c] *Department of Urology, Shanghai First People's Hospital, School of Medicine, Shanghai Jiaotong University, Shanghai 200080, P. R. China.*

[d] *Section of Nephrology, Department of Medicine, University of Chicago, Chicago, Illinois, 60637 USA. E-mail: coe@uchicago.edu*

Experimental section

Materials. The following reagents were purchased from Shanghai Chemical Reagents Co., Ltd. and without further purification: melamine (Mel, $C_3H_6N_6$, ≥99.0%), sodium hydroxide (NaOH, ≥96.0%), sodium sulfate (Na_2SO_4, ≥99.0%), potassium chloride (KCl, ≥99.5%), ammonium chloride (NH_4Cl, ≥99.5%), magnesium sulfate heptahydrate ($MgSO_4·7H_2O$, ≥99.0%), sodium chloride (NaCl, ≥99.5%), disodium hydrogen phosphate (Na_2HPO_4, ≥99.0%), sodium tartrate dihydrate ($C_4H_4Na_2O_6·2H_2O$, ≥99.0%), sodium bicarbonate ($NaHCO_3$, ≥99.5%), citric acid monohydrate ($C_6H_8O_7·H_2O$, ≥99.5%), potassium citrate monohydrate (K_3Cit, $C_6H_5K_3O_7·H_2O$, ≥99.5%), sodium dihydrogen phosphate (NaH_2PO_4, ≥99.0%), glycine ($C_2H_5NO_2$, 99.5-100.5%), histidine ($C_6H_9N_3O_2$, $[\alpha]^{20}_D$ = -38.0 ~ -42.0 °m^2/kg), serine ($C_3H_7NO_3$, $[\alpha]^{20}_D$ = +13.5 ~ +15.5 °m^2/kg), formaldehyde (CH_2O, 37-40%), sodium carboxymethycellulose (CMC-Na, 300-800), etc. Uric acid (UA, $C_5H_4N_4O_3$, ≥98.0%) and potassium oxonate (PO, $C_4H_2KN_3O_4$, ≥98.0%) were obtained from Shanghai Macklin Biochemical Technology Co., Ltd. All the above chemical reagents were of analytical grade. 3-mercaptopropionic acid (MPA, $C_3H_6O_2S$, 99%) and N-(3-Dimethylaminopropyl)-N′-ethylcarbodiimide hydrochloride (EDC, $C_8H_{17}N_3·HCl$, 98.5%) were purchased from Aladdin Reagent (Shanghai) Co., Ltd. Myoglobin from equine heart (Mb, 17.7 kDa, ≥90%) and N-hydroxysuccinimide (NHS, $C_4H_5NO_3$, ≥97%) was purchased from Sigma-Aldrich trading Co., Ltd. and lysozyme from hen egg white (LZM, 14.4 kDa, 95-100%) was obtained from Shanghai Roche Pharmaceutical Co., Ltd. 10% formalin solution and 1% CMC-Na solution were used in the experiments, and the water used was deionized.

Slow growth test. The preparation method of UA saturated solution was the same as mentioned before. Take 6 conical flasks with cover, numbered 1 to 6, respectively, 10 ml UA saturated solution was added to each flask (step ①), the following operations were performed every 24 h:

Take10 μl from each solution and observe the crystals by optical microscope (step ③). Subsequently, add 5 μl deionized water and 5 μl, 1 mM Mel solution into group 1. 5 μl, 1 mM modifier solution (sodium bicarbonate, sodium tartrate, citric acid, K_3Cit and sodium dihydrogen phosphate) and 5 μl, 1 mM Mel solution were added into group 2 to 6, respectively (step ②).

Characterization. The size, structure and morphology of the precipitate were characterized by field-emission scanning electron microscope (FE-SEM, Hitachi S-4800, Japan). Fourier transform infrared spectroscopy (FTIR, Nicolet iS10, America) and X-ray diffraction (XRD, Bruker D8, Germany) analysis to reveal the chemical structure of the obtained precipitate, element analyzer (Vario EL III, Germany) to calculate the molar ratio of UA to Mel in precipitate, the precipitate were analyzed at combustion temperatures of 1000°C, and thermogravimetric analysis (TGA, STA 409PC, Germany) was used to study the stability of the precipitate under air atmosphere at the $10°C \cdot min^{-1}$ heating rate. Ultraviolet-visible spectrophotometer (UV-vis, Agilent 8453, America) to detect the concentration of UA in solution. Optical microscope (Olympus BX51M, Japan) was used to observe the dynamic changes of crystal. Surface plasmon resonance (SPR, SR7500DC, America) measured the interaction between Mel, UA and K_3Cit.

SPR test. The SR7500DC monitored this Mel-UA, Mel-K_3Cit and UA-K_3Cit interaction in real-time with simultaneous monitoring of sample and reference channels. This experiment used 3-mercaptopropionic acid (MPA) solution self-assembled monolayer on a gold surface. The ligand, was amine coupled to the gold sheet surface with active groups using N-(3-Dimethylaminopropyl)-N′-ethylcarbodiimide hydrochloride (EDC)/N-hydroxysuccinimide (NHS) chemistry. The analyte was injected over both the sample and reference surface at a range of concentrations.

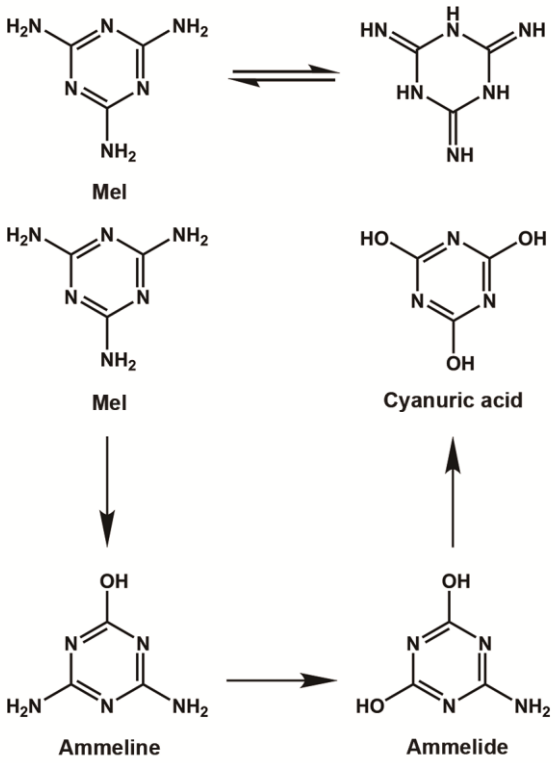

Fig. S1 Mel and its derivatives.

Illegal traders disguised Mel as protein, thereby reducing the costs of production and making illegal profits. The current method of detecting protein content is the kjeldahl method, which assesses the content of protein indirectly by measuring total nitrogen content, this scientific loophole leaves a chance for illegal traders. Mel (2, 4, 6-triamino-1, 3, 5-triazine, $C_3H_6N_6$) happens to be high in nitrogen and low in price, so it was adulterated into milk powder.

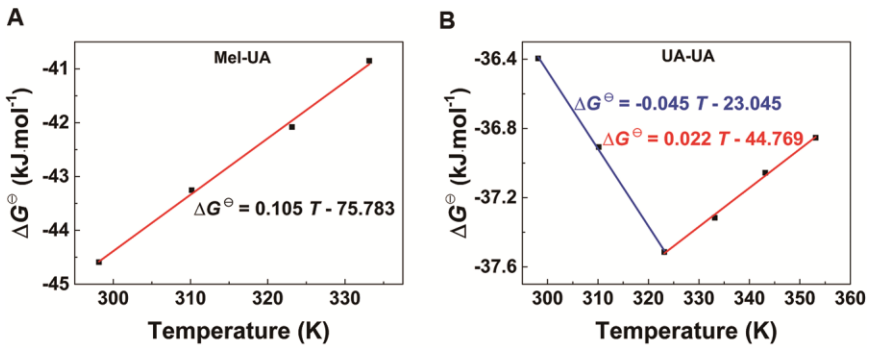

Fig. S2 Thermodynamic constant measurement. The curve of Gibbs free energy change ($\Delta G^{\ominus}$) with temperature (T): (A) UA system with Mel. (B) UA system without Mel.

Both systems have a strong reaction trend, generating stable structures.

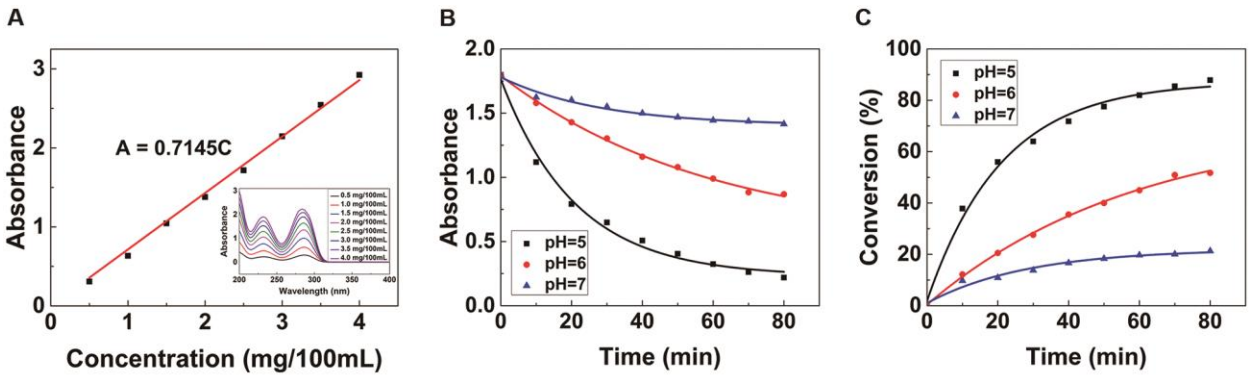

Fig. S3 Aggregation rates of UA system with Mel. (A) The standard curve of UA at λ=286 nm. (B, C) The diagrams of UV-vis absorption curves (B) and conversion rate curves (C) at different pH.

The supramolecular aggregation rate can't be expressed by conventional reaction rate constant, so we used the conversion rate to represent the aggregation rate of Mel-UA composite.

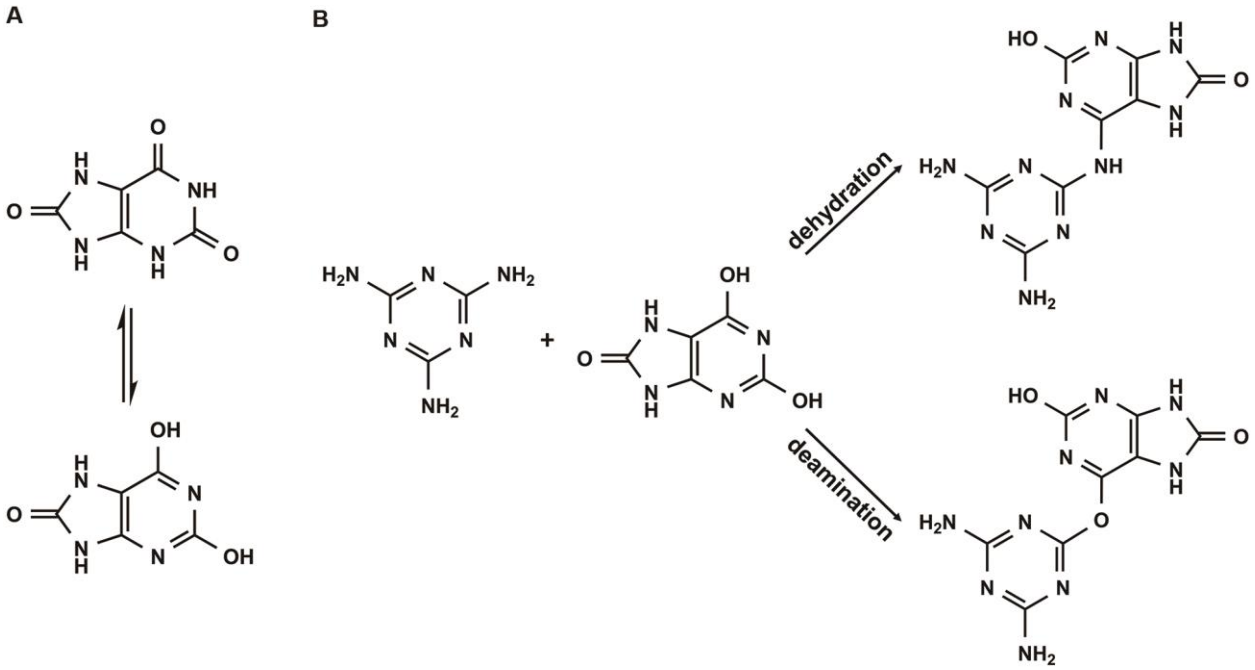

Fig. S4 (A) Tautomer of UA. (B) The two possible products after condensation reactions.

If condensation reactions occur between Mel and UA, new covalent bonds such as ether bonds are formed. However, no characteristic peaks corresponding to the new chemical bond are seen in the FTIR image of Mel-UA composite, so we believe that Mel and UA are combined by non-chemical bonds. Mel contains nine hydrogen bonding sites, including three sp^2 hybridized nitrogen atoms of triazine ring, which can act as hydrogen bonding acceptors, and six hydrogen bonding donors from the three exocyclic unsubstituted primary amine groups. UA possesses four NH and three CO sites in its tri-keto form. Therefore, Mel and UA are most likely to combine through hydrogen bonds.

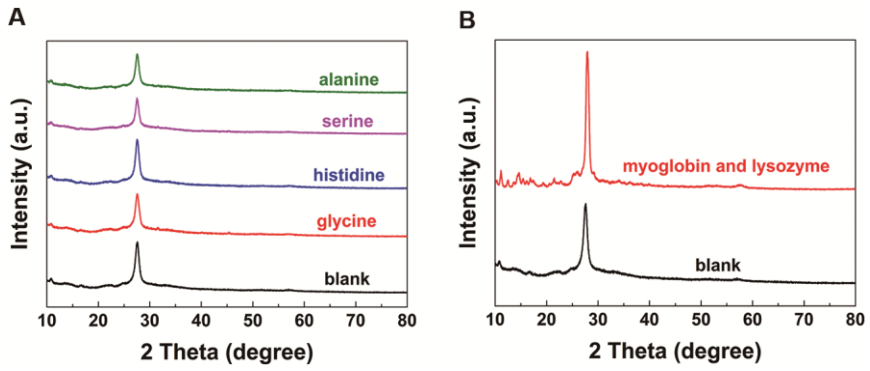

Fig. S5 XRD contrast diagrams with or without additives. (A) Additives (amino acid): glycine, histidine, serine and alanine. (B) Additives (protein): myoglobin and lysozyme.

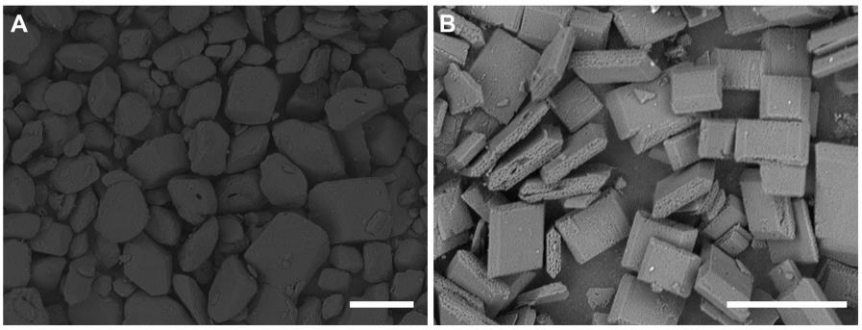

Fig. S6 SEM images of separate Mel (A) and UA (B). (scale bar = 30 μm)

The Mel-UA composite showed a dense, well-defined network of fibers, each circa 30 nm wide. As a blank experiment, the separate Mel and UA crystals obtained from supersaturated Mel and UA solution were also characterized. The pure Mel were irregular bulk aggregates, and its size distribution was uneven (A). While the microstructure of pure UA displayed bulk and uniform polyhedron which was approximate 15 μm in length and 10 μm in width (B). The morphology of the Mel-UA composite was different from that of pure Mel and UA, it suggested that Mel could combine with UA to form a new composite.

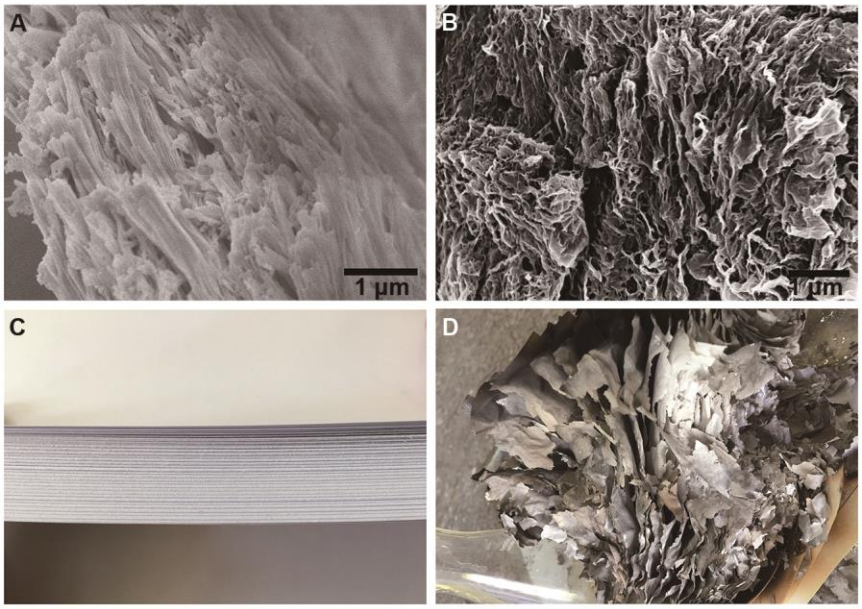

Fig. S7 Verification of layered structures. (A, B) SEM images of the Mel-UA composite before (A) and after (B) carbonization. (C, D) Photographs of A4 paper before (C) and after (D) combustion.

The Mel-UA composite exhibited a layered structure after carbonization, which was similar to a stack of burned A4 paper. Therefore, it is further proved that the composite formed by the combination of Mel and UA is a layered structure.

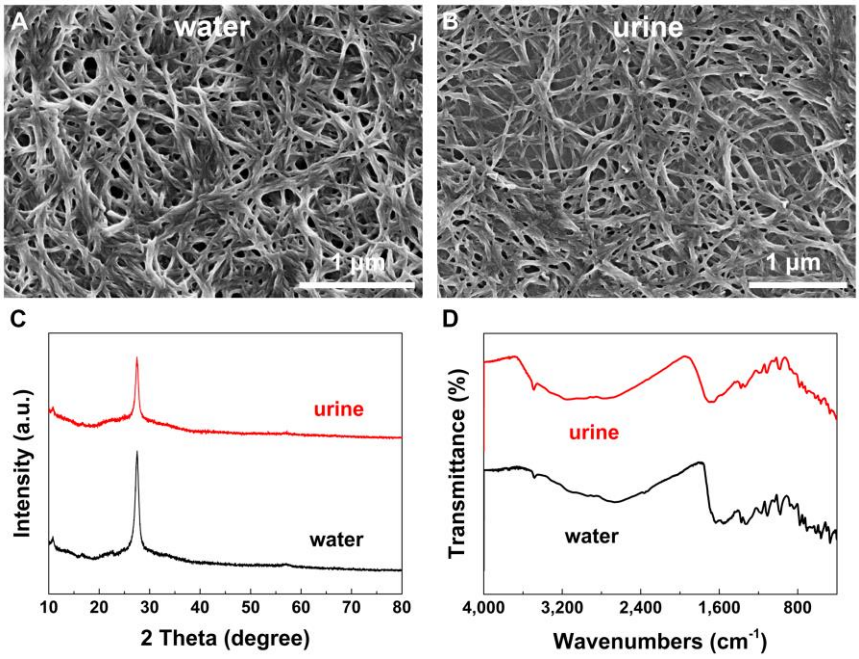

Fig. S8 Comparison of products obtained in aqueous solution and synthetic urine system. (A, B) SEM images. (C) XRD diagram. (D) FTIR spectra.

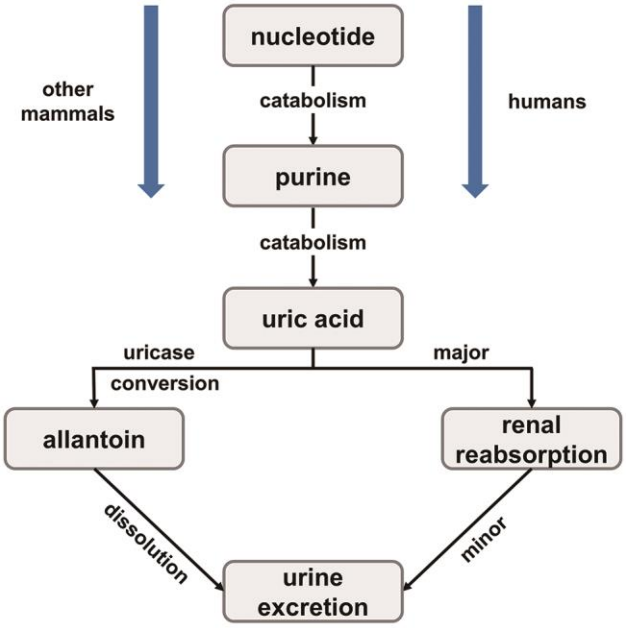

Fig. S9 Metabolism of UA in humans and other mammals.

In mice, UA is oxidized to allantoin by hepatic uricase, the solubility of allantoin is 10 to 100 times that of UA, so it can be excreted directly, Mel-UA stones seem difficult to be formed due to the low UA in urine. However, for humans who have missed the uricase activity by mutational silencing, UA is present at high levels. PO is a uricase inhibitor, PO-induced hyperuricemia in mice could serve as an ideal animal model to explore the formation mechanism of Mel-induced kidney stones. Before the study *in vivo*, a saturated solution of Mel and PO (pH were adjusted to 6) was mixed at 37.5°C for 24 h to examine if the crystals would be produced. We found no obvious crystal formation in solution.

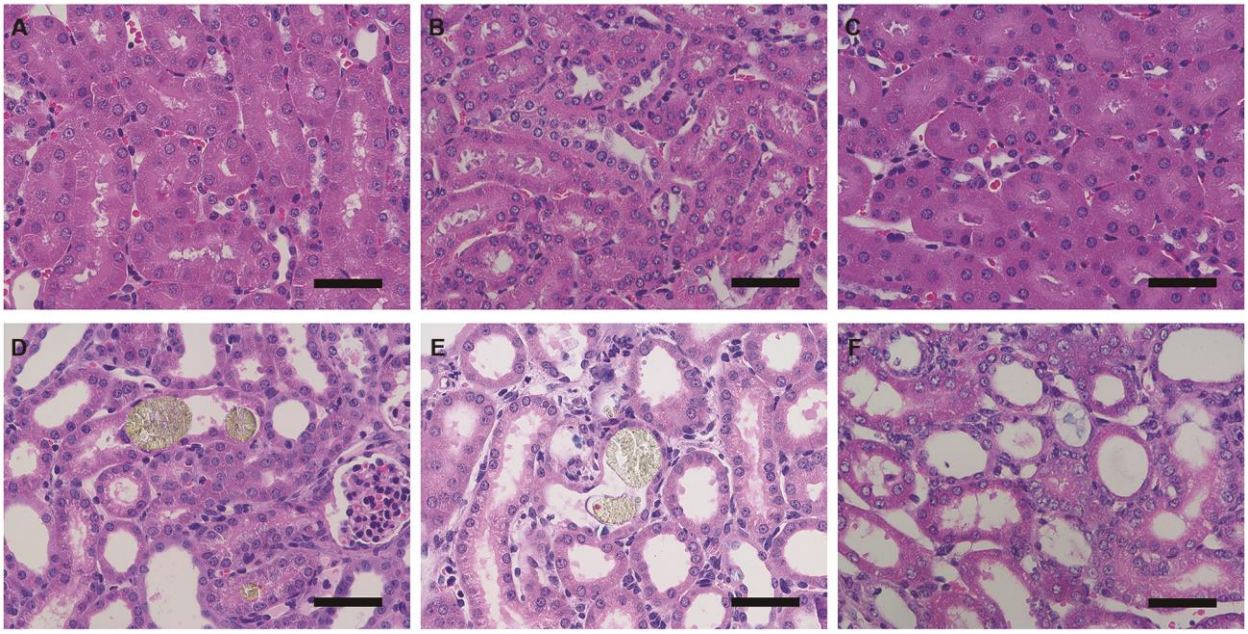

Fig. S10 Representative pathological features of kidneys in different dose groups. (A) Control group. (B) Mel alone group. (C) PO alone group. (No stone formation was seen in the renal pathological sections of A-C) (D-F) Combined dosing groups: HD, brown, dense and ellipsoidal stones were noted in the lumens of renal tubules (D); MD, the internal structure of the stones is relatively loose (E); LD, no stones were found (F). (Renal tubules were dilated in the presence or absence of stones.) (H&E staining, ×400 magnification, scale bar = 50 μm)

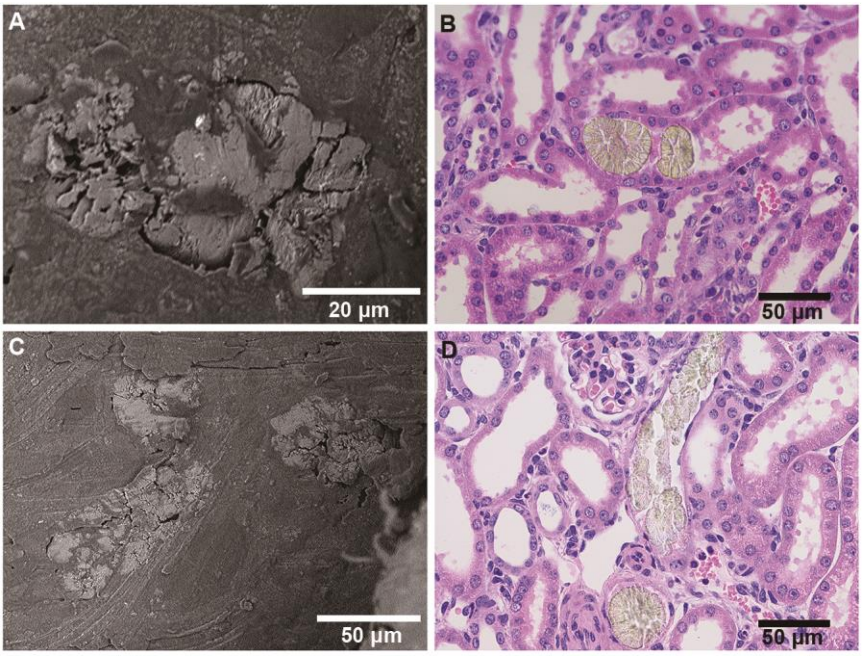

Fig. S11 Characterization of kidney sections in the stone growth group. (A, C) SEM images. (B, D) Representative pathological features (H&E staining, ×400 magnification).

We were unable to perform real-time pathological section analysis of the stones in the same mouse. Therefore, we randomly dissected 3 mice at each time period, observed the renal pathological sections, and selected the representative stone shape at this time period. Finally, according to the shape change of stones in this presumed time series, the growth process of the stones was summarized.

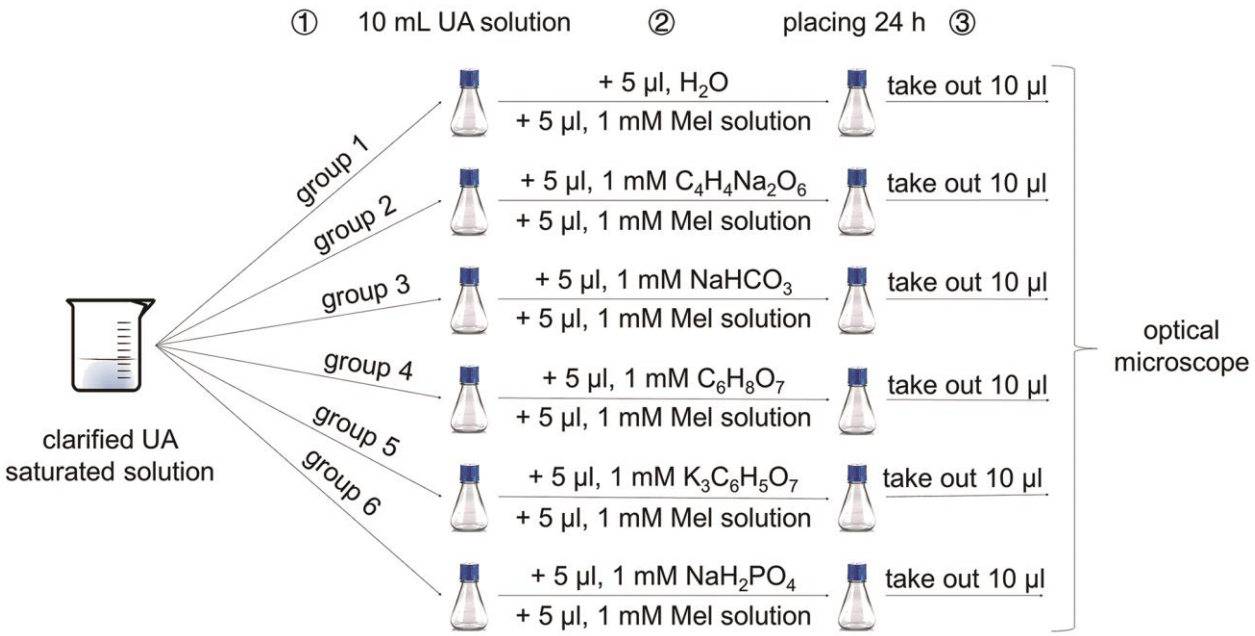

Fig. S12 The scheme of slow growth model test procedure.

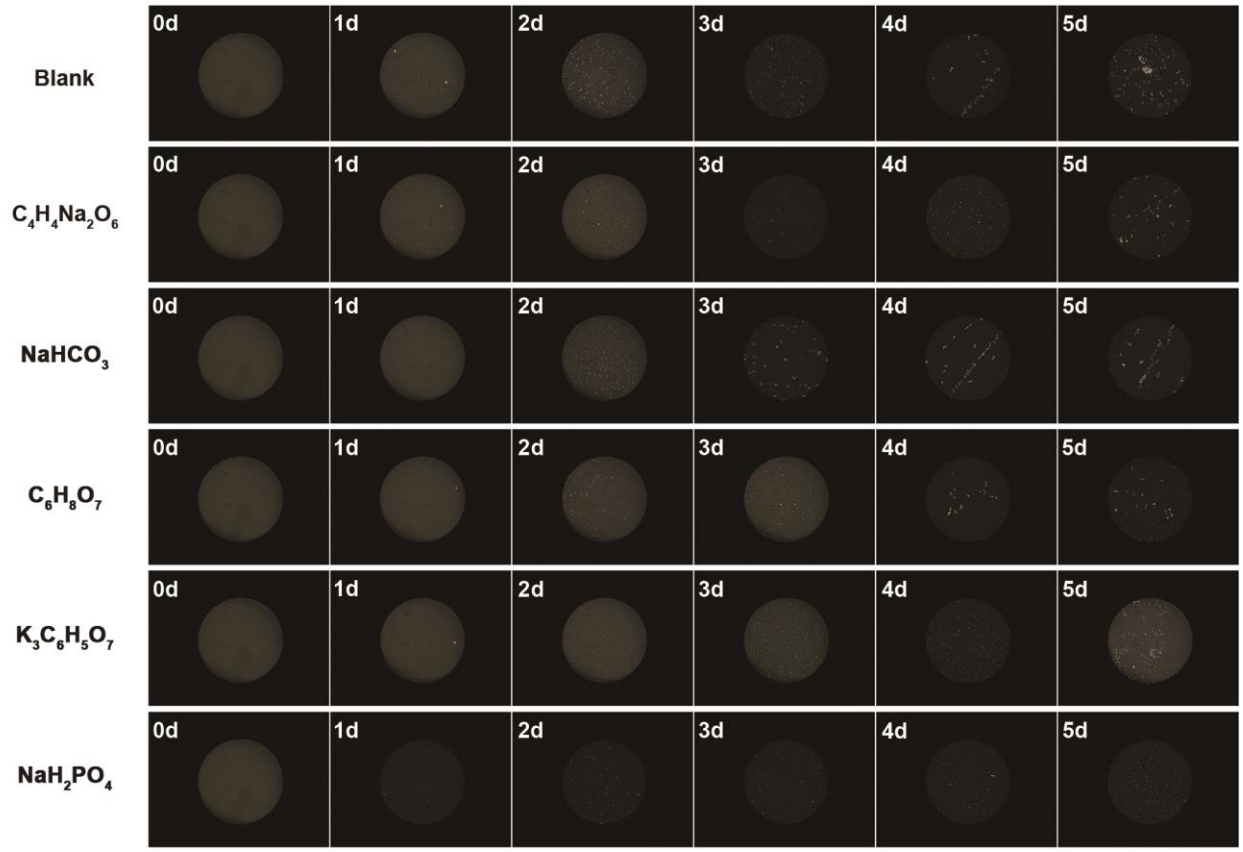

Fig. S13 Slow growth test. Dynamic changes of crystals under different regulators (blank, sodium tartrate, sodium bicarbonate, citric acid, K_3Cit and sodium dihydrogen phosphate) within five days by optical microscope.

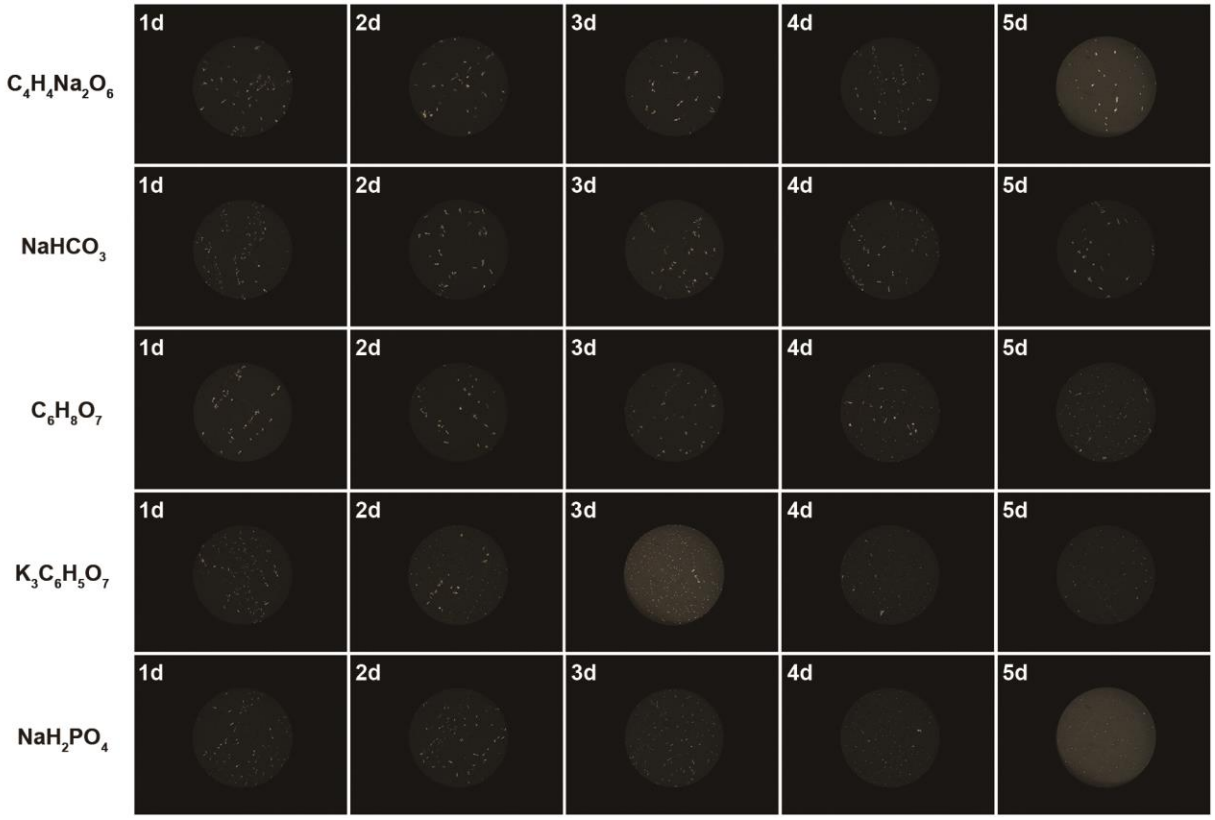

Fig. S14 Slow elimination test. Dynamic changes of crystals under different regulators (sodium tartrate, sodium bicarbonate, citric acid, K_3Cit and sodium dihydrogen phosphate) within five days by optical microscope.

In the slow growth and slow elimination tests, K_3Cit and sodium dihydrogen phosphate had the best inhibition and elimination effect on stones, but sodium dihydrogen phosphate is toxic, its median lethal dose (LD_{50}) of intraperitoneal injection was 250 mg/kg. Therefore, we chose K_3Cit for the experiments *in vivo*.

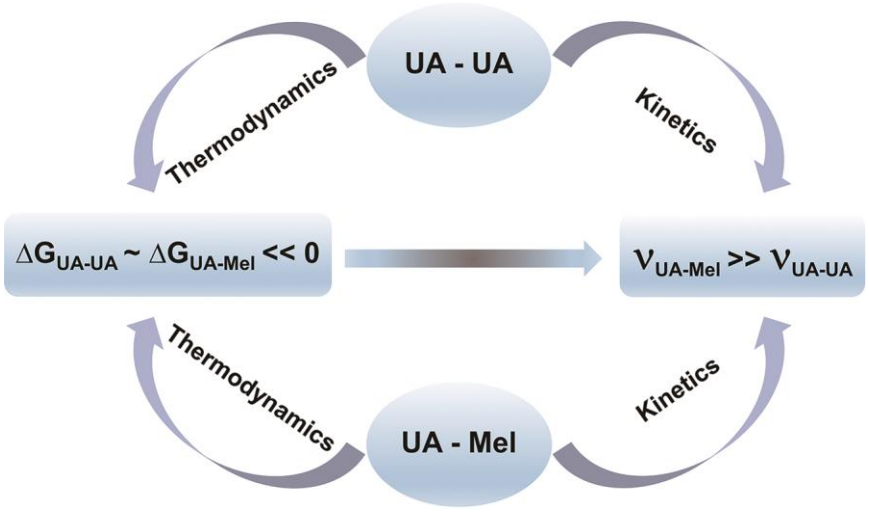

Fig. S15 Thermodynamic and kinetic analysis of the UA system with (UA-Mel) and without (UA-UA) Mel.

The formation of stones is influenced by the combination of thermodynamics and kinetics. Thermodynamics analyzes the possibility of stone formation, while kinetics studies the rate of stone formation. When the rate is slow, small crystals are easily excreted with urine and do not cause stones. When the rate is fast, small crystals grow and aggregate rapidly, blocking the renal tubules, resulting in pathological stones.

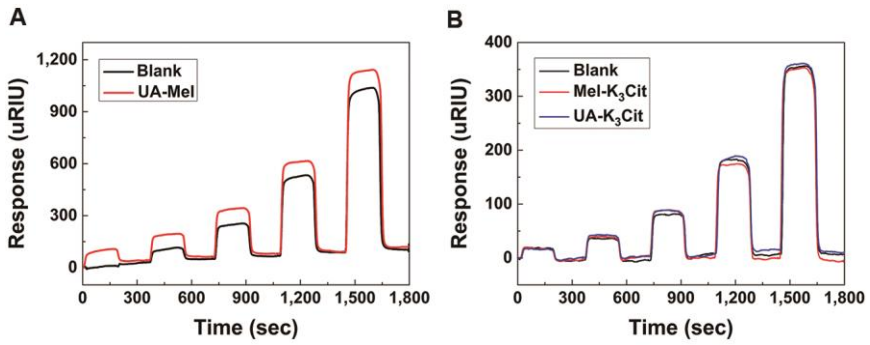

Fig. S16 SPR sensorgrams showing injections of (A) Mel at concentrations of 0.25, 0.5, 1, 2 and 4 g/L and (B) K_3Cit at concentrations of 0.16, 0.32, 0.64, 1.28 and 2.56 g/L.

The equilibrium dissociation constant (K_D) of Mel-UA, Mel-K_3Cit and UA-K_3Cit was $1.874e^{-1}$, $1.059e^{-1}$ and $2.630e^{-2}$ M, respectively.

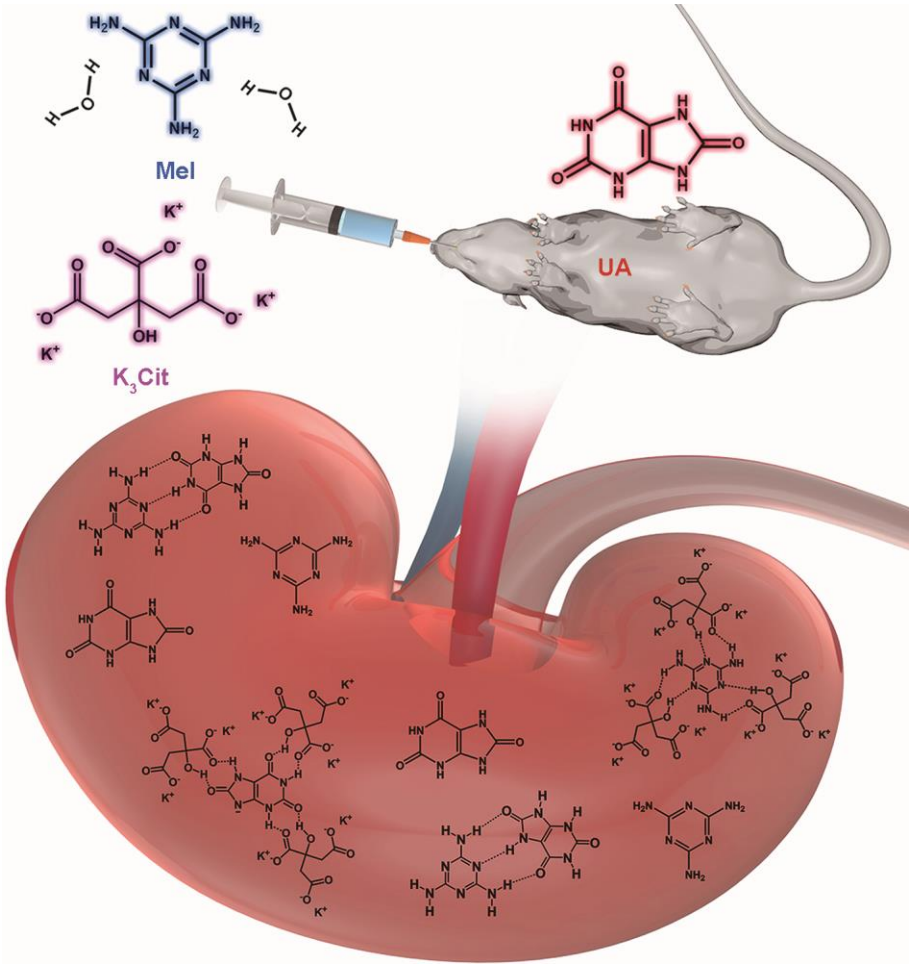

Fig. S17 Schematic diagram of K_3Cit inhibiting the formation of kidney stones. Uricase inhibitor increases UA concentration in mice, and then administer K_3Cit and Mel aqueous solution in order. K_3Cit is easier to combine with UA or Mel through hydrogen bonds to form soluble supramolecular, thereby inhibiting the combination of Mel and UA. A large number of small molecular aggregates are dispersed in the kidneys, and no insoluble supermolecule are formed. This process explained why K_3Cit could inhibit the formation of kidney stones in the experiments *in vivo* and *in vitro*.

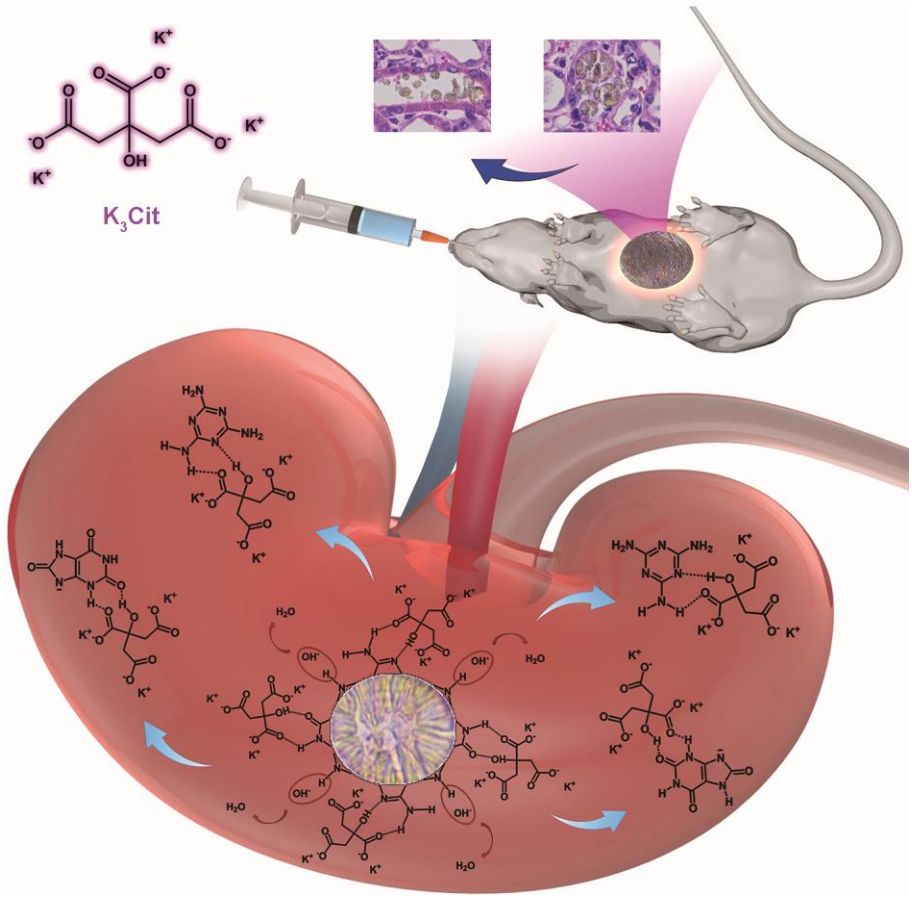

Fig. S18 Schematic diagram of K_3Cit eliminating the kidney stones. After the formation of Mel-UA stones in mice, K_3Cit was injected as a drug.

K_3Cit could associate with UA and Mel exposed to the surface of the stones, the solubility of UA and Mel increased after combined with K_3Cit, then released into solution. In this way, the K_3Cit peeled off the stones layer by layer, and dissolved the stones ultimately. This process explained why K_3Cit could eliminate the kidney stones in the experiments *in vivo* and *in vitro*.

Table S1 Composition of synthetic urine

Solution A	Concentration (mM)	Solution B	Concentration (mM)
$NaSO_4$	19.34	NaH_2PO_4	15.45
$MgSO_4 \cdot 7H_2O$	5.93	Na_2HPO_4	15.64
NH_4Cl	86.73	NaCl	223.08
KCl	162.60		

*Synthetic urine was obtained by mixing equal volumes of solutions A and B.

Table S2 Mass of white precipitate after freeze drying. (sample 1-7 represents Mel and UA at a concentration ratio of 1:5, 2:5, 1:2, 3:5, 4:5, 1:1 and 2:1, respectively)

Samples	Mass (mg)
1	0
2	0
3	30.8
4	65.4
5	91.7
6	115.9
7	118.2

As the concentration of Mel increases, the mass of the sample increases in turn. When the concentration ratio of Mel to UA is 1:1, the mass of the sample almost reaches the maximum. Continue to increase the amount of Mel, the sample mass does not change significantly. Therefore, we hypothesize that the ratio of Mel to UA is about 1:1.

Table S3 Elemental analysis of Mel-UA composite

Samples	C (%)	N (%)	C N ratio	UA: Mel (molar ratio)
1	30.83	39.58	0.78	0.9: 1
2	31.25	40.40	0.77	0.9: 1
3	30.84	39.56	0.78	0.9: 1
4	31.03	40.19	0.77	0.9: 1
5	30.92	40.17	0.77	0.8: 1
6	30.96	39.84	0.78	0.8: 1
7	31.22	40.48	0.78	0.9: 1
8	31.10	40.20	0.77	0.9: 1
9	30.96	39.85	0.78	0.9: 1
10	30.91	39.98	0.77	0.9: 1

*The molar ratio of UA to Mel was around 0.9: 1. (Samples numbered 1 to 5 were prepared by direct mixing of Mel and UA solutions, and molar ratio of Mel to UA was 1:2, 3:5, 4:5, 1:1 and 2:1, respectively. Samples numbered 6 to 10 were obtained by adding Mel to UA solution drop by drop, the molar ratio of Mel to UA was the same as before.)

This calculated data is basically close to the theoretical results and the analysis results of infant stones. However, the molar ratio of UA to Mel in infant stones ranged from 1.2: 1 to 2.1: 1. The possible reason is that small UA crystals can act as the center of crystallization to induce the formation of Mel-UA stones in the complex humoral environment, so the content of UA is higher than that of Mel in infant stones. *In vitro*, only Mel and UA interact with each other, so there are some differences with the results *in vivo*. The electronegativity of the oxygen atom is stronger than that of the nitrogen atom, thus the oxygen atom of C=O in UA is more likely to be used as a hydrogen bond acceptor, compared with nitrogen atoms of the triazine ring in Mel. Meanwhile, the positive charge on the hydrogen atom of –NH in UA is more than that of $–NH_2$ in Mel.

Therefore, when Mel combined with UA, priority to meet the hydrogen bond sites of UA, due to the presence of steric hindrance, the sites in Mel may be idle, so the proportion of Mel is higher than that of UA.

Table S4 $\Delta G^{\ominus}$, $K_{sp}^{\ominus}$ of the reaction between Mel and UA at different temperatures

Temperature (K)	[UA] (mol/L)	$K_{sp}^{\ominus}$	$\Delta G^{\ominus}$ (kJ/mol)
298.15	$1.241*10^{-4}$	$1.541*10^{-8}$	-44.590
310.15	$2.278*10^{-4}$	$5.191*10^{-8}$	-43.253
323.15	$3.969*10^{-4}$	$1.576*10^{-7}$	-42.082
333.15	$6.269*10^{-4}$	$3.930*10^{-7}$	-40.854

Table S5 Various indicators of mice after administering Mel plus PO

Mel ($mg \cdot (kg \cdot d)^{-1}$)	PO ($mg \cdot (kg \cdot d)^{-1}$)	Experimental days	Survival ratio	Kidney/body weight (%)	Mice with stones	Histological changes	stone conditions
200	400	3	3/20	2.49	1/3	+++	+++
150	300	5	9/20	2.15	9/9	+++	++
100	200	13	18/20	1.66	0/18	++	-
200	0	20	20/20	1.50	0/20	-	-
0	400	20	20/20	1.58	0/20	-	-
0	0	20	20/20	1.34	0/20	-	-

*The average values of kidney/body weight (%) were calculated by selecting three mice randomly from each group. Histological changes include hyperemia, interstitial vascular dilation, and hydropic degeneration (+++ was defined as obvious tubular dilation; ++ was defined as medium tubular dilation; + was defined as slight tubular dilation). Crystals conditions include the shape and size of crystals (+++ was defined as large and regular stones, ++ was defined as large and irregular crystals, + was defined as small crystals).

According to the Chinese Center for Disease Control and Prevention, Mel levels in the most contaminated infant formula range from 8.6 to 23.4 mg/kg body weight per day, which is approximately equivalent to a mouse dose of 71.7 - 195.0 mg/kg, so we set three different doses of Mel at 100, 150 and 200 mg/kg, respectively. PO is used to induce the increase of UA in mice, so its concentration is set as twice the concentration of Mel. In addition, to study the effects of Mel or PO on mice, we set up two control groups, the concentration of Mel and PO are 200 and 400 mg/kg (maximum concentration in the combination groups), respectively.

Table S6 Various indicators of mice in stone inhibition and elimination experiments

Experiment	K_3Cit ($mg \cdot (kg \cdot d)^{-1}$)	Experimental days	Survival ratio	Kidney/body weight (%)	Mice with stones	Histological changes	stone conditions
Inhibition	2000	10	14/20	1.60	0/14	-	-
Elimination	2000	7	10/20	1.72	0/10	+	-
Contrast	0	7	5/20	2.10	5/5	+++	+

*The average values of kidney/body weight (%) were calculated by selecting three mice randomly from each group. Histological changes include hyperemia, interstitial vascular dilation, and hydropic degeneration (+++ was defined as obvious tubular dilation; ++ was defined as medium tubular dilation; + was defined as slight tubular dilation). Crystals conditions include the shape and size of crystals (+++ was defined as large and regular stones, ++ was defined as large and irregular crystals, + was defined as small crystals).

The mortality of the mice in the inhibition group was 30%, which was significantly lower than that in the stone growth group (55%). No crystals were found in the renal pathological sections of the mice, no obvious damage was observed in the renal tubules, and there was no significant difference in the kidney/body weight between the inhibitory group and the blank control group. There were no stones in the renal pathological sections of the mice in the elimination group, indicating that the stones had been eliminated. In addition, compared to the kidney injury in the stone growth group, the injury was significantly reduced after treatment. In order to eliminate the possibility of free excretion of stones, we set up a stone elimination contrast group. After the stones were grown in the mice, no administration measures were taken. A small amount of crystals can still be seen in the renal pathological sections, but the morphology is slightly changed, and the tubular enlargement is still obvious.